Applied Physics Letters ARTICLE pubs.aip.org/aip/apl

Magnetization control of the critical current in a S-(S/F)-S superconducting switch

Cite as: Appl. Phys. Lett. **124**, 162605 (2024); doi: 10.1063/5.0202571
Submitted: 5 February 2024 · Accepted: 5 April 2024 ·
Published Online: 19 April 2024

View Online Export Citation CrossMark

Lukas Kammermeier[a] and Elke Scheer

AFFILIATIONS

Department of Physics, University of Konstanz, 78464 Konstanz, Germany

Note: This paper is part of the APL Special Collection on Josephson Junctions and Related Proximity Effects: From Basic Science to Emerging Applications in Advanced Technologies.
[a]**Author to whom correspondence should be addressed:** lukas.kammermeier@uni-konstanz.de

ABSTRACT

We show the control of the critical current I_c of a superconductor–superconductor/ferromagnet–superconductor [S-(S/F)-S] type switch by the magnetization state of the F. The inverse proximity effect of a S/F bilayer is used to define the weak link and hence the maximum critical current of the junction. The magnetization of the F lead is set by an external magnetic field. We show that the critical current in zero field depends on the remanent magnetization state via stray-field effects and thereby allows for a post-manufacturing control of the junction's properties, in particular the tunability between a maximal critical current and a full suppression of I_c without applying a persistent magnetic field. We propose a simplified model based on the relative orientation of magnetic domains that explains our findings qualitatively.

The interplay of superconductivity and ferromagnetism is a particularly interesting field of research due to the large potential of application for superconducting spintronic devices. With the ongoing development in superconducting logic devices,[1,2] also the development of nonvolatile cryogenic memory is essential. Many studies are devoted to the superconducting proximity effect by investigating spin polarized triplet generation, π junction formation, etc.[3,4] The magnetization dependence of critical currents is actively being studied in superconductor-ferromagnet-superconductor (S-F-S) junctions in which the current passes through the F layer,[5,6] clearly showing a magnetization dependence of spin triplet creation by the proximity effect and stray-field contributions in the F layer.

Other pseudo-spin-valve architectures aim to minimize switching energies between parallel or anti-parallel spin alignments to realize a memory element.[7,8]

Our present work addresses the inverse proximity effect and microscopic stray fields of a F finger affecting a S wire. The inverse proximity effect weakens the superconducting properties of the S near the S/F interface, thereby reducing the critical current I_c through the thin S in a junction. Previous works in this field achieved control via spin polarized current injection and required applied fields or increased temperature to manipulate I_c accompanied by changes in the Fraunhofer patterns of Josephson junctions[9–11] or focused on a two-state binary switch.[12,13] In this report, we show nonvolatile controllability of I_c without a persistently applied field or control current during the current–voltage transport measurements, by simply utilizing the remanent magnetization of the F, which is trained into a given magnetization state before the transport measurements are performed. Importantly, we achieve to stabilize the device's I_c at multiple values between full suppression and a maximum magnitude that exceeds the native value. Hence, with this approach, it is possible, in principle, to encode a multi-valued memory, instead of a bivalued one. It has to be noted though that the precise switching fields and exact I_c values depend on the magnetic history of the device.

The sample is a S wire made of Al with a constriction in the center with a width of $\approx$ 340 nm, length of $\approx$ 380 nm, and a thickness of 35 nm, on top of which a finger-shaped Co lead with thickness 140 nm and width $\approx$ 275 nm is placed perpendicular to the long axis of the S wire. A colored scanning electron micrograph of the junction is shown in Fig. 1. The wire's constriction needs to be sufficiently thin to allow full suppression of the superconductivity, but thick enough not to lose its superconductivity without magnetization of the F. The thicker Al leads (thickness 75 110 nm) ensure a higher critical current in the leads than in the constriction. The patterning is done by standard e-beam lithography using a bilayer mask (resist and copolymer) on an oxidized Si wafer, followed by electron-beam physical vapor deposition and a liftoff process. All metals are deposited in a single shadow evaporation process in a UHV chamber without breaking the vacuum

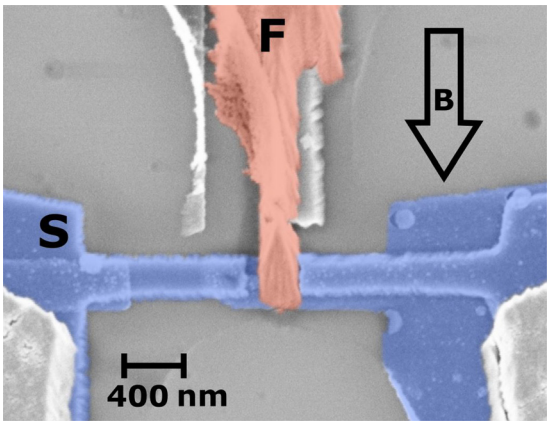

FIG. 1. False-colored electron micrograph of the S-(S/F)-S junction. The Al wire and its leads (blue) are oriented from left to right and is contacted from the top by the F cobalt electrode (red). The shadow evaporation leads to sloped edges and duplicate Al structures, which are designed to have higher critical current than the thin wire.

between the deposition of the layers to achieve the best possible metallic contact at the S/F interface. The sample is cooled by liquid nitrogen during the evaporation to avoid thermal deformation of the resist mask. We assume the Co film to be polycrystalline based on its granular surface topography, and the supplemental material contains imagery.

All measurements are performed in a dilution refrigerator at fixed sample temperature of 200 mK, if not stated otherwise. Current–voltage characteristics (IVs) and differential currents dI and voltages dV are measured in the usual four-point configuration with lock-in amplifiers. The IVs show a clear zero resistance branch up to a supercurrent I_c. The IVs are not hysteretic in terms of the current direction. The critical temperature $T_c = 0.8 \pm 0.05$ K was determined directly after the cooldown, before the sample was exposed to any applied magnetic fields.

The reduced critical temperature with respect to the critical temperature of Al of 1.17–1.2 K (Refs. 14–16) is indicative for the inverse proximity effect[17,18] and the further weakening of the superconductivity by the stray fields of the F finger. For the full sample characterization, we refer to the supplementary material. Similar data have been recorded on five samples with similar parameters. In this manuscript, we concentrate on one sample and one reference sample.

The magnetization training as sketched in Fig. 2 is organized in the following way. First, the sample is initially magnetized strongly into one direction by applying an in-plane magnetic initialization field B_{init} along the axis of the F lead of −2 T. Transport measurements are performed after the external field is ramped down to 0 mT again. Next, a training field B_{train} (of 0–300 mT) is applied into the opposite direction of the initialization field, and the field is ramped to zero again. Exclusively, at zero applied field, the transport measurement is performed. This second step is then repeated for many training fields, increasing in absolute field size each step. Thereby, the magnetization is step by step inverted from the initial direction into the direction of the training field.

In the following figures, the quantity B_{train} refers to the last training field seen by the sample, not a persistently applied field. In the state "$B_{\text{train}} = 0$ mT," the sample has been exposed to the initialization field $B_{\text{init}} = -2$ T, but no training field in the other direction, leaving the sample in the fully magnetized initial state. Continuing with higher training fields, the sample has then experienced all previous training fields. $B_{\text{train}} = 20$ mT, for example, refers to the state after applying −2 T, 0, 10, and 20 mT and is now again at 0 mT applied field to be measured.

The transport measurements have the typical IV-characteristics of a superconducting wire, see Fig. 3. The applied bias current I causes no voltage drop across the junction as long as its absolute value is smaller than the critical current I_c. At the point where $|I| > I_c$, the transport properties become dissipative and a voltage drop is measured. This is reflected in the differential resistance $dR = dV/dI$ as a peak at the critical current I_c, where the transport properties change from superconducting to normal conducting and vice versa.

The color map in Fig. 3(c) presents dR vs I as the function of B_{train} increased from 0 to 300 mT in 10 mT steps. We observe a strong dependence of the critical current I_c on B_{train}. At $B_{\text{train}} = 0$ mT, the ferromagnet remains in its fully magnetized initial state of $B_{\text{init}} = -2$ T, fully suppressing the S transport through the junction. In this exemplary dataset after $B_{\text{train}} = 20$ mT, the sample jumps in a configuration that supports a finite supercurrent again. Step by step increasing B_{train} influences I_c only slightly in a range from $B_{\text{train}} = 20$ to $B_{\text{train}} = 130$ mT, before for larger B_{train}, it decreases again reaching full suppression at $B_{\text{train}} = 230$ mT. Above this training field, only a slight nonlinearity of the IV remains to even higher B_{train}, but no zero-resistance state is achieved anymore.

Our hypothesis to explain these findings is that I_c follows the magnitude of the remanent magnetization M of the F finger. We therefore interpret the data as magnetization dependent critical current $I_c(M)$, leading to a suppressed superconductivity in strongly magnetized states and a recovery of superconductivity whenever the absolute magnetization is small.

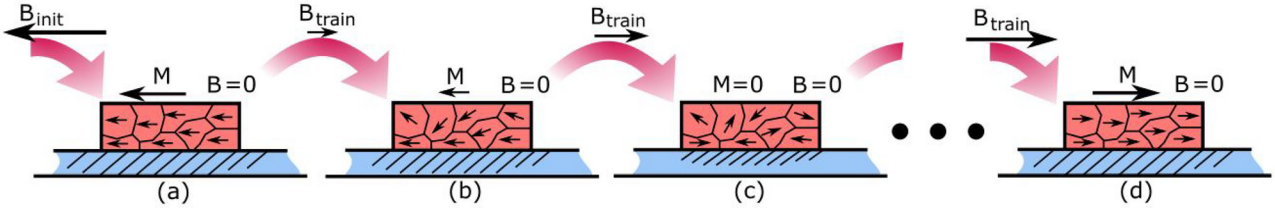

FIG. 2. Sketch of the magnetization procedure. (a) A initialization field B_{init} is applied to start in a fully magnetized state of the ferromagnet (red). (b) and (c) By applying increasingly strong opposite training fields B_{train}, the magnetization is reduced and the I_c suppression of the superconductor (blue) is reduced, until at some point F is again strongly magnetized in the direction opposite to the initialization (d). In between the training stages, the applied field B is reduced to zero for the transport measurements.

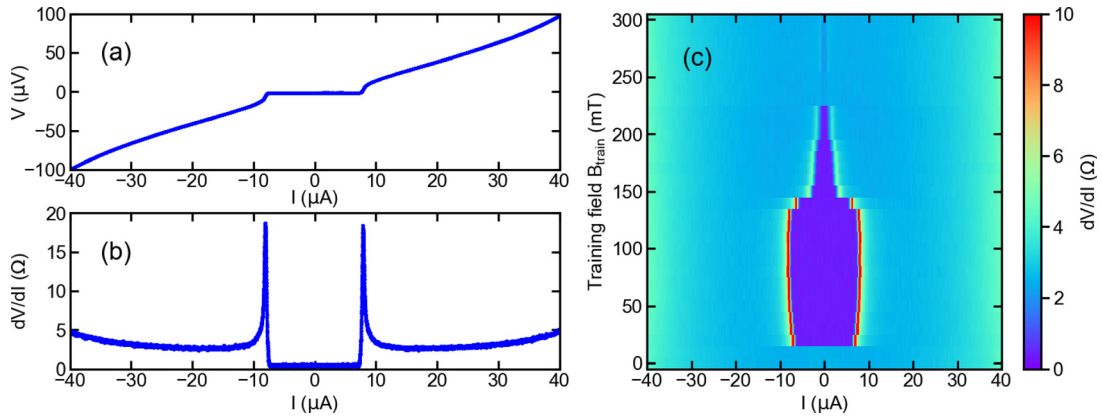

FIG. 3. (a) Voltage V vs current I characteristic of the junction in a state of low magnetization after $B_{train} = +100$ mT training, showing superconductive transport. (b) The corresponding lock-in measured differential resistance dR vs current I. (c) B_{train} dependent color map of the dR vs I measurements with $B_{init} = 2$ T.

A similar behavior is also observed in a corresponding measurement in the opposite field direction shown in Fig. 4 with an initialization now in the positive field direction $B_{init} = +2$ T. It is to be mentioned that the detailed position and amplitude of the I_c steps is not reproducible. Each magnetization dependent map shows variations in the maximum amplitude of I_c and the training fields at which jumps in I_c are observed. Some examples of $I_c(B_{train})$ behavior are shown in Fig. 5. The I_c values shown are extracted at the peak positions of the dR vs I plot. The general trend (full suppression for $B_{train} = 0$ mT, maximum I_c around $B_{train} \approx 100$–200 mT, full suppression again above ≈ 250 mT, and the formation of I_c-plateaus) is observed in all traces, independent of the step width that varied from 1 to 20 mT. In some traces (e.g., the red and the gray curves in Fig. 5), a second full suppression of I_c is observed around $B_{train} \approx 60$ 70 mT.

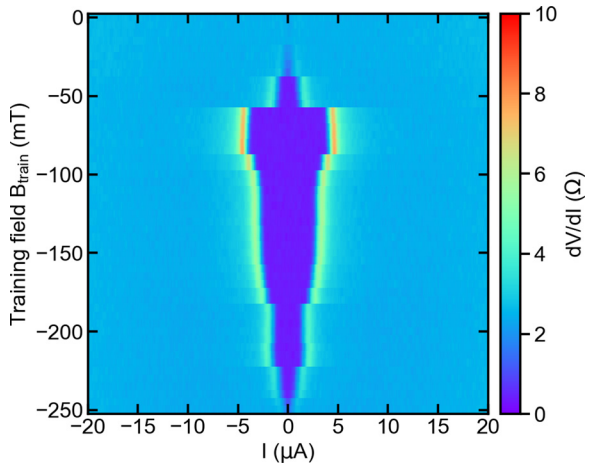

FIG. 4. Magnetization dependent dR vs I color map, analogous to Fig. 3(c), but now initialized in the opposite field direction with $B_{init} = +2$ T.

Hence, the I_c jumps are attributed to domain depinning events and are closely connected to the Barkhausen jumps[19] in ferromagnets. We assume that individual or few domains change their orientation after a certain B_{train} threshold resulting in a significantly different stray-field configuration influencing the S. We attribute the larger jumps to domains at the S/F interface since their closer proximity should have a stronger impact on the resulting stray field change. Also, the statistical variations in the jump positions and heights between individual measurements fit within this model, assuming that the F domains form in slightly different orientations and positions in each training cycle.

To address the question whether the magnetization dependent suppression mechanism is caused by the inverse proximity effect or the magnitude of the stray field around the ferromagnetic finger, we performed reference measurements on a sample with identical dimensions, but an additional AlO_x layer between the Al and Co to prevent the short ranged proximity effect or ferromagnetic exchange interactions. The critical temperature of the reference sample is $T_{c,ref} = 1.05 \pm 0.05$ K much higher than the one of the sample

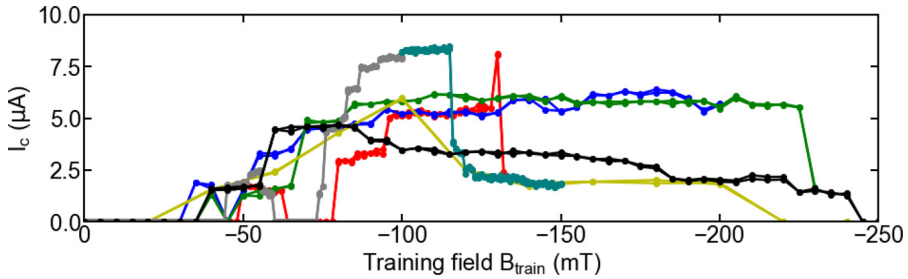

FIG. 5. Multiple I_c vs B_{train} plots of the same sample show significantly varying shapes. The black datapoints are extracted from the data of Fig. 4. The datapoints are connected by lines for clarity.

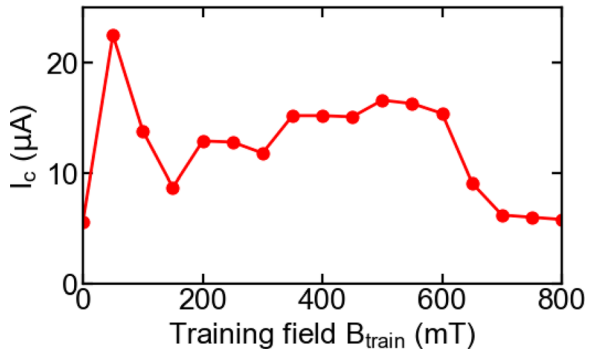

FIG. 6. Exemplary I_c vs B_{train} of the reference sample with oxidized S/F interface showing magnetization dependence. Further information in the supplementary material. T = 950 mK and $B_{init} = \quad 3T$.

without oxide barrier, signaling that the inverse proximity effect contributed markedly to the reduced T_c of the first sample. Another indication for the inverse proximity effect in the first sample is the much higher $I_{c,\mathrm{ref}}$ of the reference sample, see Fig. 6. In addition, the IVs of the reference sample are hysteretic showing a retrapping current $I_{r,\mathrm{ref}} < I_{c,\mathrm{ref}}$, see the supplementary material for more details.

Despite the much higher absolute $I_{c,\mathrm{ref}}$, it can still be controlled by the magnetization state of the F finger. These results show, on the one hand, that the inverse proximity effect is relevant for the overall properties of the device and, on the other hand, that the control mechanism is dominated by the stray fields of the F, which themselves depend on its magnetization state. To be specific, we suggest that I_c is controlled by the stray field inside the S finger. Areas in which this field size overcomes the critical field B_c, switch to the normal state, thereby reducing the resulting I_c. This mechanism implies that the external B field can enter the S also locally. This is possible in type II superconductors and in type I superconductors in the mixed state. Al as a bulk material is a type I superconductor; however, thin disordered Al films as investigated here are usually type II and therefore allow for field entering the wire. To confirm this, we analyze the magnetic field dependence of the IVs (see Fig. S4 in the supplementary material), from which we can extract a field penetration depth of $\approx 300 \quad 400$ nm, which is an order of magnitude larger than the sample thickness.

In summary, we have observed a clear influence of the magnetic history of a ferromagnet onto the critical current of a thin superconducting junction in proximity. We interpret the findings as a local suppression of superconductivity due to the stray field, reducing the critical current of the junction in a controllable way, in addition to the inverse proximity effect limiting the maximal I_c. The absolute suppression is a combination of both effects reducing I_c. We argue that the controllability is caused by stray fields, but a M-dependent inverse proximity could contribute to the reduction of I_c. Jumps in $I_c(B_{\mathrm{train}})$ are attributed to magnetic domain flips, changing the stray-field distribution, resulting in general in a weaker suppression and hence higher I_c in states of low magnetization. This enables the nonvolatile controlled manipulation of one of the most relevant junction parameters I_c, after manufacturing and without persistent external control fields. Micromagnetic simulations to test these interpretations are under way.

See the supplementary material for temperature dependencies of the main sample and reference sample, as well as a more detailed discussion of the reference samples' fabrication and transport properties; an atomic force micrograph of the Co surface topography of the main sample; and the estimation of the coherence length ξ_D and penetration depth λ based on magnetic field dependent data.

We acknowledge the use of the experimental equipment and the expert support concerning its usage provided by the Nanostructure Laboratory at the University of Konstanz.

This work was financially supported by the Deutsche Forschungsgemeinschaft (DFG, German Research Foundation) - Projektnummer 317077841.

AUTHOR DECLARATIONS

Conflict of Interest

The authors have no conflicts to disclose.

Author Contributions

Lukas Kammermeier: Conceptualization (equal); Data curation (lead); Formal analysis (lead); Visualization (lead); Writing – original draft (lead); Writing – review & editing (equal). **Elke Scheer:** Conceptualization (equal); Project administration (lead); Supervision (lead); Writing – review & editing (equal).

DATA AVAILABILITY

The data that support the findings of this study are available from the corresponding author upon reasonable request.

REFERENCES

[1]G. Yang, C. Ciccarelli, and J. Robinson, "Boosting spintronics with superconductivity," APL Mater. **9**, 050703 (2021).
[2]J. Linder and J. W. A. Robinson, "Superconducting spintronics," Nat. Phys. **11**, 307–315 (2015).
[3]A. I. Buzdin, "Proximity effects in superconductor-ferromagnet heterostructures," Rev. Mod. Phys. **77**, 935 (2005).
[4]M. Eschrig, "Spin-polarized supercurrents for spintronics: A review of current progress," Rep. Prog. Phys. **78**, 104501 (2015).
[5]K. Lahabi, M. Amundsen, J. A. Ouassou, J. Linder, J. Aarts *et al.*, "Controlling supercurrents and their spatial distribution in ferromagnets," Nat. Commun. **8**, 2056 (2017).
[6]R. Fermin, N. M. A. Scheinowitz, J. Aarts, and K. Lahabi, "Mesoscopic superconducting memory based on bistable magnetic textures," Phys. Rev. Res. **4**, 033136 (2022).
[7]B. Baek, W. Rippard, S. Benz, S. Russek, and P. Dresselhaus, "Hybrid superconducting-magnetic memory device using competing order parameters," Nat. Commun. **5**, 3888 (2014).
[8]N. Satchell, P. Shepley, M. Algarni, M. Vaughan, E. Darwin, M. Ali *et al.*, "Spin-valve Josephson junctions with perpendicular magnetic anisotropy for cryogenic memory," Appl. Phys. Lett. **116**, 022601 (2020).
[9]O. Vávra, W. Pfaff, and C. Strunk, "Planar S-(S/F)-S Josephson junctions induced by the inverse proximity effect," Appl. Phys. Lett. **95**, 062501 (2009).
[10]O. Vávra, W. Pfaff, R. Monaco, M. Aprili, and C. Strunk, "Current-controllable planar S-(S/F)-S Josephson junction," Appl. Phys. Lett. **102**, 072602 (2013).
[11]J. Fan, B. Jiang, J. Zhao, R. Bi, J. Zhou, Z. Liu, F. Qu, L. Lu, X. Wu *et al.*, "Homointerface planar Josephson junction based on inverse proximity effect," J. Appl. Phys. **131**, 093903 (2022).
[12]T. W. Clinton and M. Johnson, "Magnetoquenched superconducting valve," J. Appl. Phys. **83**, 6777–6779 (1998).

[13]T. W. Clinton, P. R. Broussard, and M. Johnson, "Advances in the development of the magnetoquenched superconducting valve: Integrated control lines and a Nb-based device," J. Appl. Phys. **91**, 1371–1377 (2002).
[14]J. F. Cochran and D. E. Mapother, "Superconducting transition in aluminum," Phys. Rev. **111**, 132 (1958).
[15]B. T. Matthias, T. H. Geballe, and V. B. Compton, "Superconductivity," Rev. Mod. Phys. **35**(1), 1 (1963).
[16]C. Kittel, *Introduction to Solid State Physics* (John Wiley & Sons, Inc., New York, 2005).
[17]S. Mironov, A. S. Mel'nikov, and A. Buzdin, "Electromagnetic proximity effect in planar superconductor-ferromagnet structures," Appl. Phys. Lett. **113**, 022601 (2018).
[18]J. Xia, V. Shelukhin, M. Karpovski, A. Kapitulnik, and A. Palevski, "Inverse proximity effect in superconductor-ferromagnet bilayer structures," Phys. Rev. Lett. **102**, 087004 (2009).
[19]R. M. Bozorth and J. F. Dillinger, "Barkhausen effect. III. Nature of change of magnetization in elementary domains," Phys. Rev. **41**, 345 (1932).